Available online at www.sciencedirect.com
SCIENCE DIRECT®
International Journal of Mass Spectrometry 238 (2004) 1–15
International Journal of Mass Spectrometry
www.elsevier.com/locate/ijms

Ab initio study of the isomerization and photodissociation of the $C_3H_6O^{+\bullet}$ cation radicals

K. Mishima[a,*], M. Hayashi[b], S.H. Lin[a]

[a] *Institute of Atomic and Molecular Sciences, Academia Sinica, P.O. Box 23-166, Taipei 10764, Taiwan, Republic of China*
[b] *Center for Condensed Matter Sciences, National Taiwan University, Taipei 106, Taiwan, Republic of China*

Received 2 July 2003; accepted 6 August 2004
Available online 11 September 2004

Abstract

We have performed ab initio (using Gaussian-2 (G2M) method) calculations for the reactant, intermediates, transition states, and photofragmentation products of the $C_3H_6O^{+\bullet}$ cation radicals in order to elucidate its unimolecular photofragmentation and isomerization mechanisms. We have identified nine photofragmentation pathways, 39 stable intermediates, and 61 transition states for the acetone cation radical $CH_3COCH_3^+$ as an initial state by ab initio calculations. The isomerization pathways among them are also characterized. It was found that the photofragmentation and isomerization pathways are intertwined through various transition states. Two of the nine pathways contain only one transition state with high energy (70–80 kcal/mol) just after the reactant. In the other ones, the reactant acetone cation radical is transformed into an enol structure via one transition state, and enol and ether isomers undergo many-step isomerizations. From the ab initio calculation, the reaction pathways found in this work have energy barriers higher than those obtained by Heinrich et al. [J. Am. Chem. Soc. 110 (1988) 8183]. In general, the photofragmentation species not investigated previously are found to have high energies, which coincides with the fact that the previous experiments conducted with low laser intensity and short wavelength do not reveal such species.

Keywords: Ab initio calculation; $C_3H_6O^{+\bullet}$ cation radical; Isomerization; Photodissociation

1. Introduction

Molecular ionization and dissociation in intense laser fields have attracted much attention in recent years due to the advent of high power lasers. Because of this, it is essential to investigate theoretically in detail high-energy chemical species which are expected to play some roles in the high-power laser experiments.

Among experimentalists and theoreticians, there has been much interest in unimolecular dissociations of polyatomic cations in the gas phase [1,2]. For example, two photodissociation channels of the acetone cation radical via α-bond cleavage (Norrish type I),

$$CH_3COCH_3^+ \rightarrow CH_3CO^+ + CH_3 \quad \text{and}$$
$$CH_3COCH_3^+ \rightarrow CH_2CO^+ + CH_4, \qquad (1.1)$$

have been experimentally investigated in detail in the literature [2]. In particular, the reaction (1.1) is well documented in [3]. Heinrich et al. [4] and Ceno et al. [5] have conducted detailed ab initio and RRKM calculations to elucidate methyl loss and methane elimination in unimolecular fragmentations of the acetone cation radical (1.1). Their emphasis lies on the existence of hydrogen-bridged complexes as intermediates for the reaction paths, which were verified by the ab initio calculation. Using the Keldysh parameter [6,7], it is found that all these studies are in the multiphoton ionization region. Even recently, there has also been an experimental study with a 355 nm laser pulse [8]. It was not a multiphoton region in which this experiment was performed; instead, it was a sequential ionization study. The maximum laser intensity used in this study was 3×10^9 W/cm^2. This is five orders of magnitude below the electric field intensity given in [4,5]. The lasers in this study were not focused so that the intensity is much lower than when the lasers are focused.

* Corresponding author. Tel.: +886 223644261; fax: +886 223620200.
E-mail address: mishima@gate.sinica.edu.tw (K. Mishima).

1387-3806/$ – see front matter © 2004 Elsevier B.V. All rights reserved.
doi:10.1016/j.ijms.2004.08.003

However, Wu et al. [9] published interesting experimental results in the high power, low frequency incident laser region, which reveal novel photofragmentation products not found in the low intensity laser experiments cited above. The Keldysh parameter γ is estimated to be unity [6,7], which means that their photoionization experiment is in the middle of the multiphoton and tunneling ionization regions. They calculated laser power dependence of the ion yield by a tunneling ionization model and obtained good agreement with the experimental data. However, they did not assign various peaks of their time-of-flight mass spectroscopic data that were not observed in the previous experimental results. In our opinion, in the range where $\gamma = 1.0$, the multiphoton and tunneling ionizations compete and it will not be adequate to use only the tunneling ionization model. Their experimental results indicate that only the methyl loss and methane elimination are not sufficient to elucidate the photofragmentation mechanisms. Our calculational results reveal that the acetone cations require much higher energies to overcome the potential barriers for the isomerization pathways other than the methyl loss and methane elimination. In other words, it is natural that only the methyl loss and methane elimination have been observed in the photofragment products in low intensity laser experiments.

The purpose of the present paper is to elucidate the mechanism of the photodissociation processes and rearrangements after the ionization of the acetone cation radical theoretically by using ab initio calculation. We shall show the dissociation and isomerization pathways not previously reported in detail. To the best of our knowledge, there has been no comprehensive theoretical study on the isomerization and dissociation of the acetone cation radical except for [10]. It may be very important to investigate in detail the photofragmentation and isomerization pathways of this molecule, because much attention of the researchers is focused on the tunneling and field ionization phenomena of polyatomic molecules in high-power laser fields [11]. In addition, the importance of studying the acetone cation radical is that it is the simplest ketone and benchmark for multiple dissociation with two equivalent bonds. For simplicity, in this study we do not take into account the unimolecular decomposition of product ions other than the parent ion. In this paper, we report new isomerization and photodissociation pathways other than those discussed, for example, by Heinrich et al. [4].

2. Calculation method

The geometries of equilibrium and transition states reported in this work have been optimized by the hybrid density functional B3LYP method [12] with the 6-31G* basis set. The harmonic frequencies were calculated at the B3LYP/6-31G* level for characterizing the stationary points and transition states, and obtaining the zero-point energy (ZPE) correction without scaling. The local minima and the transition states were identified by checking that the harmonic frequencies are all positive in the former case and in the latter case that they have only one negative eigenvalue. The energies reported in this paper are calculated at the G2M(cc, MP2) method [13], a modification of the Gaussian-2 (G2) method proposed by Pople and co-workers [14] and include the ZPE corrections. The basis sets for G2M(cc, MP2) calculations are 6-311G** for CCSD(T), 6-311 + G(3df, 2p) and 6-311G** for MP2 calculations. The symmetry of all of the species is C_1 throughout the present paper. The GAUSSIAN 98 package was employed for the ab initio calculations [15].

3. Results and discussion

From the ionization experimental results of acetone cation radical conducted with a 800 nm, 50 fs, 9.2×10^{13} (W/cm^2) laser pulse in Fig. 1(a) of [9], the singly charged ions detected by the linear time-of-flight mass spectrometer are likely to be composed of the following ions between the tunneling and multiphoton regimes:

$$H^+, C^+, CH^+, CH_2{}^+, CH_3{}^+, H_2O^+, C_2H_2{}^+, C_2H_3{}^+, C_2H_4{}^+, CO^+, C_2H_5{}^+, COH^+, CH_4O^+, C_2H_2O^+, C_2H_3O^+, C_2OH_6{}^+. \quad (3.1)$$

The ionization potential for the acetone molecule is estimated to be 224.7 kcal/mol including ZPE at the G2M(cc, MP2) level. It should be noted that the addition of a carbonyl group to an alkane decreases the ionization potential substantially [16].

On the other hand, our ab initio calculation shows that the following nine photodissociation pathways are accessible with seven to ten photons under the condition of the wave-

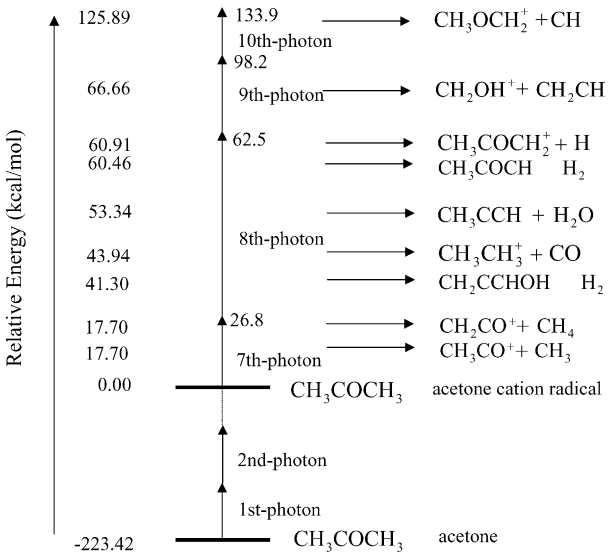

Fig. 1. Energy diagram of photoionization of acetone, acetone cation radical, and photofragmentation products of acetone cation radical at 800 nm, 50 fs, 9.2×10^{13} (W/cm^2) incident laser pulse of [9].

Table 1
Total energies, relative energies ΔE with respect to the reactant ST1, and zero-point energies (ZPE) of intermediates of acetone cation radical $CH_3COCH_3^+$ at the G2M(cc, MP2) computational level

Species		Energy (G2M(cc, MP2)) (hartree)	ΔE (kcal/mol)	ZPE (kcal/mol)
CH_3COCH_3	ST0	−192.828	−224.685	52.756
$CH_3COCH_3^+$	ST1	−192.472	0.000	51.487
$CH_3COHCH_2^+$	ST2	−192.488	−8.881	52.703
$CH_3CCHOH_2^+$	ST3	−192.414	35.786	50.574
$CH_2CH_2CHOH^+$	ST4	−192.460	9.346	53.057
$CH_2CH_2CHOH^+$	ST5	−192.422	33.859	53.549
$CH_3COHCH_2^+$	ST6	−192.487	−7.847	52.592
$CH_2CH_2CHOH^+$	ST7	−192.451	13.485	51.467
$CH_2CHCH_2OH^+$	ST8	−192.434	25.653	53.061
$CH_2OHCHCH_2^+$	ST9	−192.404	42.799	51.662
$CH_3CH_2COH^+$	ST10	−192.436	24.126	52.331
$CH_3CH_2COH^+$	ST11	−192.438	21.985	52.216
$CH_3OCHCH_2^+$	ST12	−192.467	5.121	53.075
$CH_3OCHCH_2^+$	ST13	−192.462	8.064	53.112
$CH_3CHOCH_2^+$	ST14	−192.448	15.475	51.655
$CH_3OCHCH_2^+$	ST15	−192.390	53.662	52.842
$CH_3CHCHOH^+$	ST16	−192.483	−4.698	53.179
$CH_3COCH_3^+$	ST17	−192.444	18.801	52.300
$CH_3OCHCH_2^+$	ST18	−192.390	53.100	52.838
$CH_2CHCH_2OH^+$	ST19	−192.437	22.150	51.243
$CH_2OHCHCH_2^+$	ST20	−192.403	43.530	51.481
$CH_2CHCH_2OH^+$	ST21	−192.429	27.019	50.914
$CH_3CHCHOH^+$	ST22	−192.487	−7.162	53.245
$CH_3CCH_2OH^+$	ST23	−192.396	46.249	49.627
$CH_3CHCHOH^+$	ST24	−192.486	−7.056	53.110
$CH_3CHCHOH^+$	ST25	−192.483	−5.279	53.093
$CH_2CHCH_2OH^+$	ST26	−192.435	24.922	53.089
$CH_2CH_2CHOH^+$	ST27	−192.457	11.195	52.984
$CH_3OHCCH_2^+$	ST28	−192.389	53.466	52.561
$CH_3OHCHCH^+$	ST29	−192.393	49.930	51.563
$CH_2CHCH_2OH^+$	ST30	−192.433	24.278	51.127
$CH_2CH_2CHOH^+$	ST31	−192.457	11.196	52.984
$CH_3CHOCH_2^+$	ST32	−192.447	16.257	51.944
$CHCCH_3OH_2^+$	ST33	−192.399	42.561	48.244
$CHCH_2CH_2OH^+$	ST34	−192.365	64.217	48.235
$CH_3CCH_2OH^+$	ST35	−192.395	46.955	49.865
$CH_3OHCHCH^+$	ST36	−192.393	50.346	51.798
$CH_3CH_2COH^+$	ST37	−192.444	18.785	52.496
$CH_3CH_2CHO^+$	ST38	−192.449	14.067	51.040
$CH_3CH_3OC^+$	ST39	−192.397	41.525	45.782

length 800 nm as in [9]:

$$CH_3COCH_3^+ \rightarrow CH_3CO^+ + CH_3 \quad (3.a)$$

$$CH_3COCH_3^+ \rightarrow CH_2CO^+ + CH_4 \quad (3.b)$$

$$CH_3COCH_3^+ \rightarrow CH_2CCHOH^+ + H_2 \quad (3.c)$$

$$CH_3COCH_3^+ \rightarrow CH_2OH^+ + CH_2CH \quad (3.d)$$

$$CH_3COCH_3^+ \rightarrow CH_3CH_3^+ + CO \quad (3.e)$$

$$CH_3COCH_3^+ \rightarrow CH_3CCH^+ + H_2O \quad (3.f)$$

$$CH_3COCH_3^+ \rightarrow CH_3COCH^+ + H_2 \quad (3.g)$$

$$CH_3COCH_3^+ \rightarrow CH_3OCCH_2^+ + H \quad (3.h)$$

$$CH_3COCH_3^+ \rightarrow CH_3OCH_2^+ + CH \quad (3.i)$$

These are schematically shown in Fig. 1. We have identified 39 stable intermediates, 61 transition states, and nine photodissociation pathways by ab initio calculation. We summarize the important features of all of the reaction paths (3.a)–(3.i). It should be noted that all of these reactions are isomerizations via a stepwise mechanism except (3.a) and (3.g) and one of the reaction channels corresponding to (3.b).

Tables 1–3 list energetics of the intermediates, transition states, and photofragmentation products, respectively. Table 4 shows the relative energies of the photofragmentation pathways of (3.a)–(3.i). We can see that since we have used a high calculation level, all of the total energies obtained in this work are much lower than those of Bouma et al. using the RHF/STO-3G or RHF/4-31G level of theory [17] and those of Bouchoux et al. using the PMP2/6-311+G**//MP2/6-31G* level of theory [10]. The intermediates and transition states consist of ionized enols

Table 2
Total energies and relative energies ΔE with respect to ST1 at the G2M(cc, MP2) computational level, and zero-point energies (ZPE) and imaginary vibrational frequencies ν of transition states of acetone cation radical $CH_3COCH_3^+$ at the B3LYP/6-31G* computational level

Species		Energy (G2M(cc, MP2)) (hartree)	ΔE (kcal/mol)	ZPE (kcal/mol)	ν (cm^{-1})
$CH_3COCH_3^+$	TS1	−192.410	36.016	48.567	1931.496*i*
$CH_3COH_2CH^+$	TS2	−192.363	65.241	48.022	2195.666*i*
$CH_2CHOHCH_2^+$	TS3	−192.380	56.006	49.459	478.220*i*
$CH_2CH_2CHOH^+$	TS4	−192.398	47.070	51.764	806.960*i*
$CH_2CHOHCH_2^+$	TS5	−192.357	72.139	51.380	795.380*i*
$CH_2OHCHCH_2^+$	TS6	−192.295	108.203	48.443	254.648*i*
$CH_2CH_2CHOH^+$	TS7	−192.398	46.979	51.496	866.636*i*
$CH_2CH_2CHOH^+$	TS8	−192.446	16.652	51.836	233.261*i*
$CH_3COHCH_2^+$	TS9	−192.392	47.956	49.066	2043.559*i*
$CH_2COHCH_3^+$	TS10	−192.404	43.119	50.954	354.170*i*
$CH_3CH_2COH^+$	TS11	−192.341	76.330	45.421	1743.998*i*
$CH_3CHOCH_2^+$	TS12	−192.346	73.940	45.849	1304.507*i*
$CH_4COCH_2^+$	TS13	−192.375	58.034	47.693	387.639*i*
$CH_3COCH_3^+$	TS14	−192.333	80.078	44.078	567.732*i*
$CH_3CHCHOH^+$	TS15	−192.481	−4.158	52.998	149.024*i*
$CH_3CHCHOH^+$	TS16	−192.463	7.604	52.957	277.605*i*
$CH_3CHOCH_2^+$	TS17	−192.403	41.773	49.710	1794.480*i*
$CH_3OCHCH_2^+$	TS18	−192.431	26.601	52.048	446.350*i*
$CH_3OCHCH_2^+$	TS19	−192.375	60.906	51.133	707.461*i*
CH_4CCHOH^+	TS20	−192.327	87.502	47.440	786.672*i*
$CH_3CHCHOH^+$	TS21	−192.406	42.757	52.522	442.532*i*
$CH_2CHCH_2OH^+$	TS22	−192.431	24.920	50.265	772.711*i*
$CH_3CHOCH_2^+$	TS23	−192.374	59.226	48.813	2168.257*i*
$CH_3COCH_3^+$	TS24	−192.349	72.137	45.981	518.140*i*
$CH_3COCH_3^+$	TS25	−192.443	19.136	52.109	123.588*i*
$CH_3OCHCH_2^+$	TS26	−192.387	54.358	52.574	157.621*i*
$CH_3OCHCH_2^+$	TS27	−192.388	52.239	50.063	1408.350*i*
$CH_3OCHCH_2^+$	TS28	−192.331	85.431	48.375	1997.845*i*
$CH_3OHCHCH^+$	TS29	−192.320	92.119	47.675	916.959*i*
$CH_3OCCH_3^+$	TS30	−192.228	148.901	46.919	636.557*i*
$CH_2CHCH_2OH^+$	TS31	−192.427	29.071	51.949	180.401*i*
$CH_2CHCH_2OH^+$	TS32	−192.427	28.948	52.253	236.871*i*
$CH_2CHOHCH_2^+$	TS33	−192.331	84.341	46.991	1845.267*i*
$CH_2CHOHCH_2^+$	TS34	−192.383	56.029	51.245	627.616*i*
$CH_2CHOCH_3^+$	TS35	−192.375	61.134	51.511	808.489*i*
$CH_2CHCH_2OH^+$	TS36	−192.424	30.694	51.758	190.849*i*
$CH_2CHCH_2OH^+$	TS37	−192.427	27.281	50.411	900.134*i*
$CH_3CHCHOH^+$	TS38	−192.456	10.104	51.393	982.648*i*
$CH_2CHCH_2OH^+$	TS39	−192.383	54.126	49.798	949.938*i*
$CH_3CCH_2OH^+$	TS40	−192.341	78.858	48.071	1550.123*i*
$CH_2CH_2CHOH^+$	TS41	−192.435	22.599	50.807	1012.944*i*
$CH_3CCH_2OH^+$	TS42	−192.395	46.530	49.459	391.919*i*
$CH_3CHCHOH^+$	TS43	−192.456	10.045	51.265	1001.203*i*
$CH_2CHCH_2OH^+$	TS44	−192.413	37.205	51.398	1008.599*i*
$CH^2CH_2CHOH^+$	TS45	−192.427	27.411	50.580	1077.024*i*
$CH_2CHCH_2OH^+$	TS46	−192.413	37.202	51.509	286.588*i*
$CH_3CHCHOH^+$	TS47	−192.450	14.343	51.764	619.161*i*
$CH_2CH_2CHOH^+$	TS48	−192.436	22.703	51.596	874.319*i*
$CH_2CH_2CHOH^+$	TS49	−192.451	15.028	52.995	450.878*i*
$CH_3OCH_2CH^+$	TS50	−192.360	71.181	52.112	343.265*i*
$CH_2CH_2CHOH^+$	TS51	−192.427	27.418	50.582	1074.581*i*
$CH_2OCHCH_3^+$	TS52	−192.415	35.164	50.489	403.557*i*
$CH_3OHCHCH^+$	TS53	−192.391	50.778	51.440	83.051*i*
$CHCCH_3OH_2^+$	TS54	−192.400	42.598	48.567	145.013*i*
$CH_2CHCH_2OH^+$	TS55	−192.384	53.796	49.786	920.539*i*
$CH_3OHCHCH^+$	TS56	−192.345	76.462	47.955	371.764*i*
$CHCH_2CH_2OH^+$	TS57	−192.374	60.677	50.556	656.836*i*
$CH_3CHCHOH^+$	TS58	−192.448	15.569	51.463	849.976*i*
$CH_3CH_2COH^+$	TS59	−192.435	23.800	52.065	156.823*i*
$CH_3CH_2COH^+$	TS60	−192.415	35.160	50.625	1023.216*i*
$CH_3CH_2CHO^+$	TS61	−192.383	54.228	48.745	2149.847*i*

Table 3
Total energies at the G2M(cc, MP2) computational level and zero-point energies (ZPE) of photofragmentation products of acetone cation radical $CH_3COCH_3^+$ at the B3LYP/6-31G* computational level

Species		Energy (G2M(cc, MP2)) (hartree)	ZPE (kcal/mol)
CH_3CO^+	FR1	−152.680	28.101
CH_3	FR2	−39.756	18.709
CH_2CO^+	FR3	−152.007	19.686
CH_4	FR4	−40.432	28.372
CH_2CCHOH^+	FR5	−191.224	37.619
H_2	FR6	−1.171	6.366
CH_2OH^+	FR7	−114.614	25.526
CH_2CH	FR8	−77.748	23.047
$CH_3CH_3^+$	FR9	−79.238	42.678
CO	FR10	−113.155	3.157
CH_3CCH^+	FR11	−116.049	33.139
H_2O	FR12	−76.330	13.283
CH_3COCH^+	FR13	−191.192	37.007
$CH_3OCCH_2^+$	FR14	−191.854	45.185
H	FR15	−0.500	0.000
$CH_3OCH_2^+$	FR16	−153.858	43.422
CH	FR17	−38.408	4.005

$CH_3CHCHOH^+$, distonic ions $[CH_2CH_2CHOH]^+$, ionized allyl alcohols $[CH_2CHCH_2OH]^+$. Different from [10], ionized propanal $[CH_3CH_2CHO]^+$ is not reported in this work. In Fig. 2, we show the molecular geometries of acetone molecule in the ground state, and those of reactant, intermediates, transition states, and dissociation products of the reactant, acetone cation radical.

One of the reaction pathways for (3.a) and (3.b), respectively, methyl- and methane-loss by the α-cleavage, has been described by ab initio calculations by Heinrich et al. [4], and numerous experimental studies have been concentrated on these pathways; we have found that they have the lowest energies among all the photodissociation pathways (3.a)–(3.i). One reason for this is that the acetyl ion is stable due to the electron sharing involving a nonbonding orbital of a heteroatom [16],

$$CH_3{-}\overset{+}{C}{=}O \leftrightarrow CH_3{-}C{\equiv}\overset{+}{O}.$$

Table 4
Photofragmentaion pathways and relative energies ΔE with respect to ST1 of acetone cation radical $CH_3COCH_3^+$ at the G2M(cc, MP2) computational level

Reaction		ΔE (kcal/mol)
$CH_3CO^+ + CH_3$	(3.a)	17.690
$CH_2CO^+ + CH_4$	(3.b)	17.710
$CH_2CCHOH^+ + H_2$	(3.c)	41.296
$CH_2OH^+ + CH_2CH$	(3.d)	66.660
$CH_3CH_3^+ + CO$	(3.e)	43.945
$CH_3CCH^+ + H_2O$	(3.f)	53.342
$CH_3COCH^+ + H_2$	(3.g)	60.462
$CH_3OCCH_2^+ + H$	(3.h)	67.821
$CH_3OCH_2^+ + CH$	(3.i)	125.890

However, we have found isomerization pathways different from those found by Heinrich et al. [4], although the photofragmentation products found in this study are identical with those by Heinrich et al. ((3.a) and (3.b)); they have higher intermediate energies. For example, ST17 in Fig. 6 undergoes carbon–carbon bond rupture to yield the same photodissociation products as (3.a) as shown later.

Next, we consider the second lowest barrier for the reaction shown in Fig. 3. The reactant has a potential energy barrier of 36.06 kcal/mol in this case: twice or thrice higher than those of the dissociation pathways for (3.a) and (3.b) discussed by Heinrich et al. [4]. A hydrogen atom migrates from the methyl group to the oxygen atom (ST1 → TS1 → ST6) and the enol cation radicals ST6 and ST2 are linked via the transition state TS9 by a 1,3-hydrogen shift, the energy of the enol tautomer of ST2 being lower than that of ST6 only by 1.04 kcal/mol. The structural difference between ST6 and ST2 is that the hydrogen atom of the hydroxy group is closer to the methylene group than to the methyl group in ST6 while the reverse holds in ST2. Note that the direct isomerization pathway from 2 of [4] or ST1 to 1 of [4] or ST2 through TS1/2 of [4] or TS1 has not been obtained on the computational level of the present work; instead, the transition state TS1 or TS1/2 of [4] connects the reactant ST1 or 2 of [4] with ST6 which is slightly different from ST2 or 1 of [4]. That is, the reaction pathway from ST1 or 2 of [4] to ST2 or 1 of [4] is not direct through only one transition state; instead, it involves two transition states TS1 and TS9 and one intermediate state ST6. This seems to be more reasonable.

ST2 has the lowest energy of isomers of the acetone cation radical found in this work, which is consistent with [17]. This is characteristic of radical cations, in contrast to neutral species [4,18]. Here, it should be emphasized that a variety of isomers and photodissociation products stem from the intermediates ST2 and ST6 in Fig. 3, which Heinrich et al. [4] did not investigate in detail. In particular, as will be clear later on, the transition state TS1 plays a key role for almost all of the dissociation pathways found in this work.

Next, we investigated the dissociation pathway from the reactant ST1 to the dissociation products (3.d) in Fig. 3. Hydrogen atom migrates from carbon atom to oxygen atom (ST1 → TS1 → ST6) as discussed above, and the hydrogen atom of the methyl group migrates from C^1 to C^2 to produce TS3 and the methylene group of C^2 of TS3 transfers to C^1 site (ST6 → TS3 → ST4). The dihedral angles of $O–C^1–C^2–C^3$ of ST6, TS3, and ST4 are 180.000, 136.600, and 97.463°, respectively. Therefore, since the dihedral angle of TS3 is in the middle of those of ST6 and ST4, it is clear that TS3 mediates the isomerization between ST6 and ST4. This has been also checked by the IRC calculation. Following the isomerization pathway ST4 → TS4 → ST5, a "quasi-four-membered" cyclic compound ST5 is produced. At the level of the present calculation, C^3 and oxygen atom are not tightly bonded. The dihedral angles of $O–C^2–C^1–C^3$ of ST4, TS4, and ST5 are −97.463, −28.741, and −9.531°, respectively. This indicates that ST5 has a nearly planar structure with re-

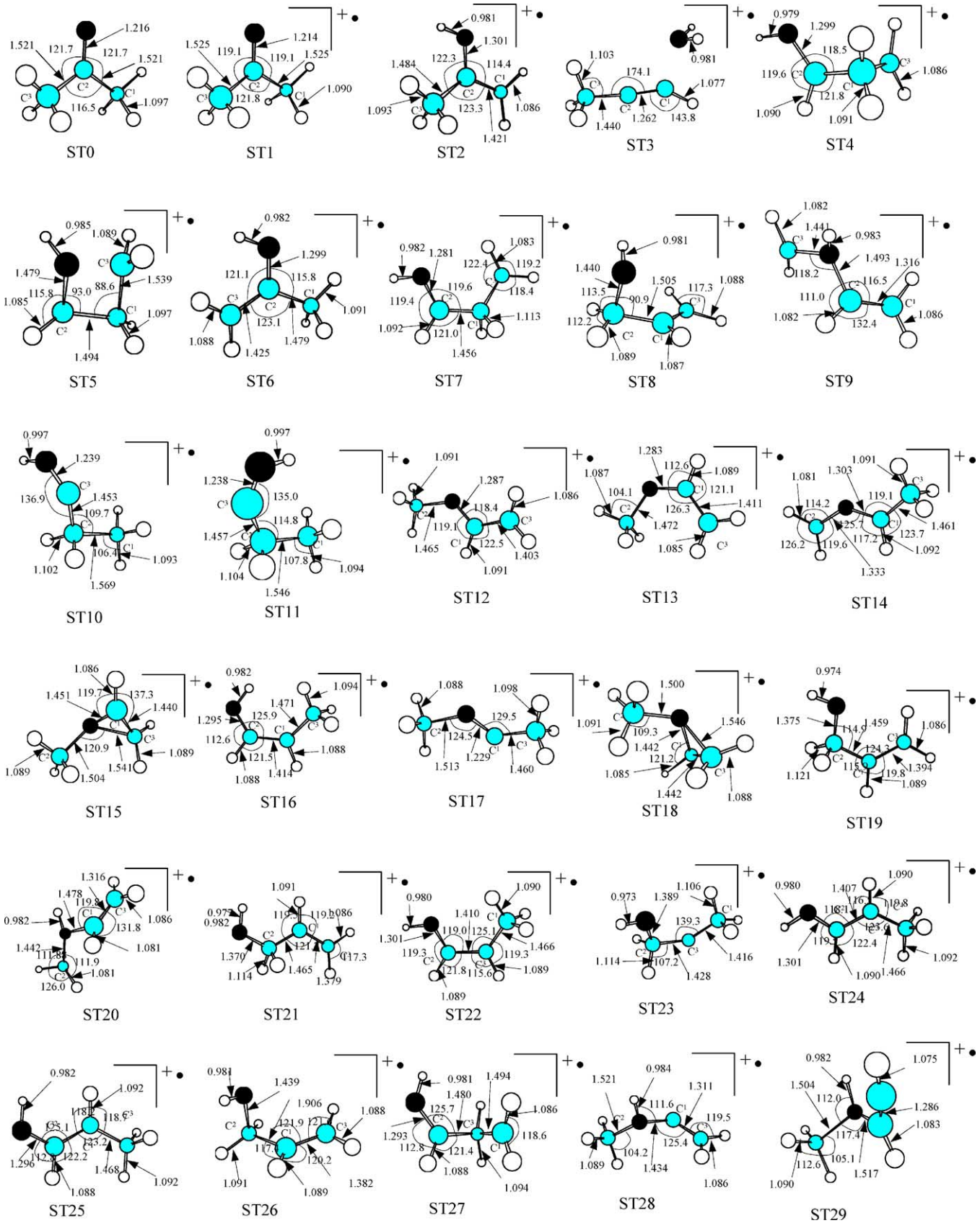

Fig. 2. Geometries of acetone (ST0), and the reactant, intermediates, transition states, and products of acetone cation radicals optimized at the B3LYP/6-31G* level. Bond lengths and bond angles are in Å and degrees, respectively. Black, gray, and white spheres indicate oxygen, carbon, and hydrogen atoms, respectively.

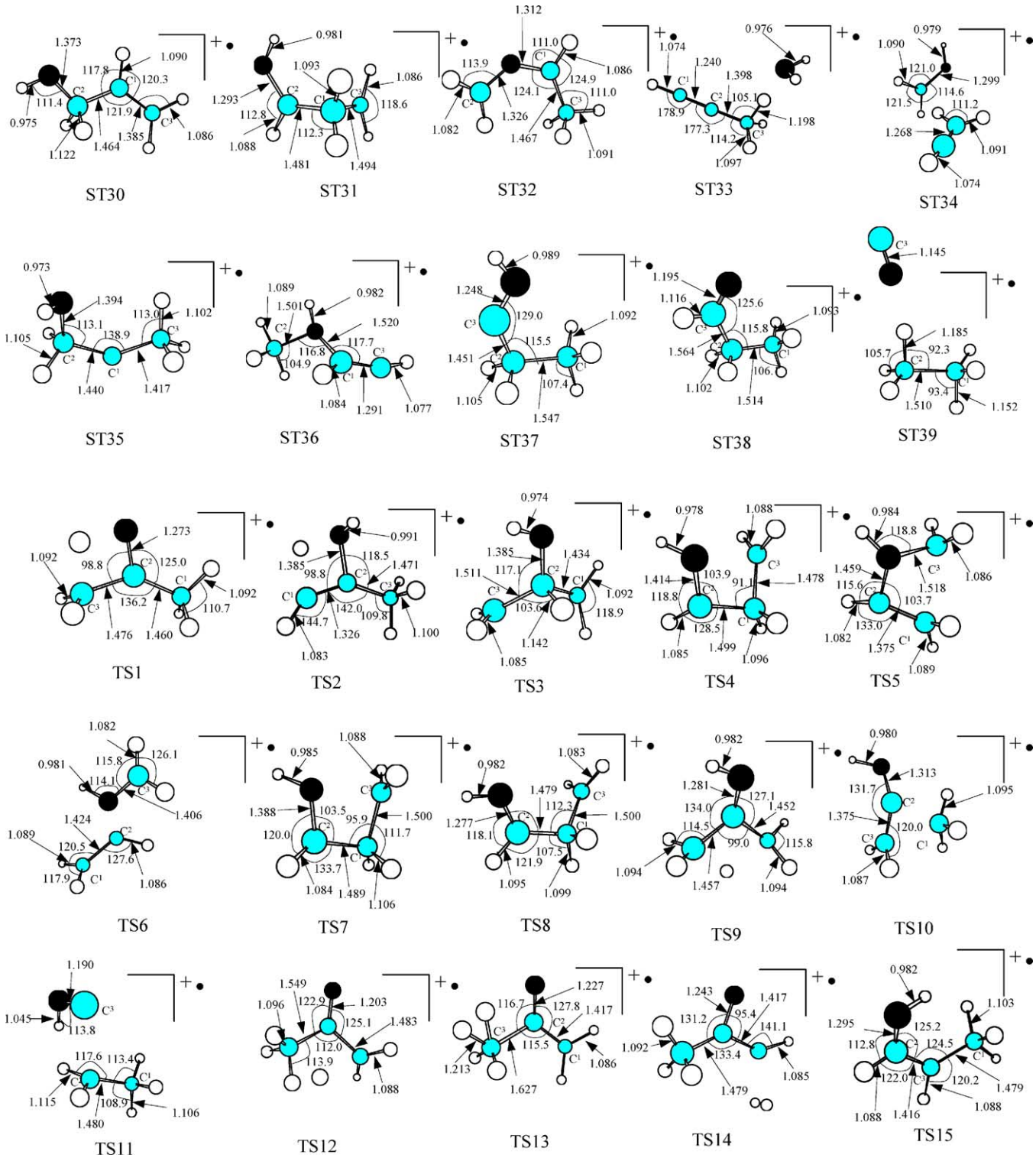

Fig. 2. (*Continued*)

gard to the skeleton. The energy of ST5 is higher than that of ST4 by 24.51 kcal/mol because of the existence of the strain energy of the ring for ST5. Then, the bond breaking between C^1 and C^3 of ST5 occurs to form TS5 which leads to the formation of C^2–O bonding (ST9). Subsequently, the elongation of C^2–O bond takes place to form the transition state TS6, which easily undergoes fragmentation. Because the potential energy barrier of TS6 is quite high (108.20 kcal/mol), it is clear that the photofragmentation pathway (3.d) will hardly contribute to the production of the photofragments of (3.d).

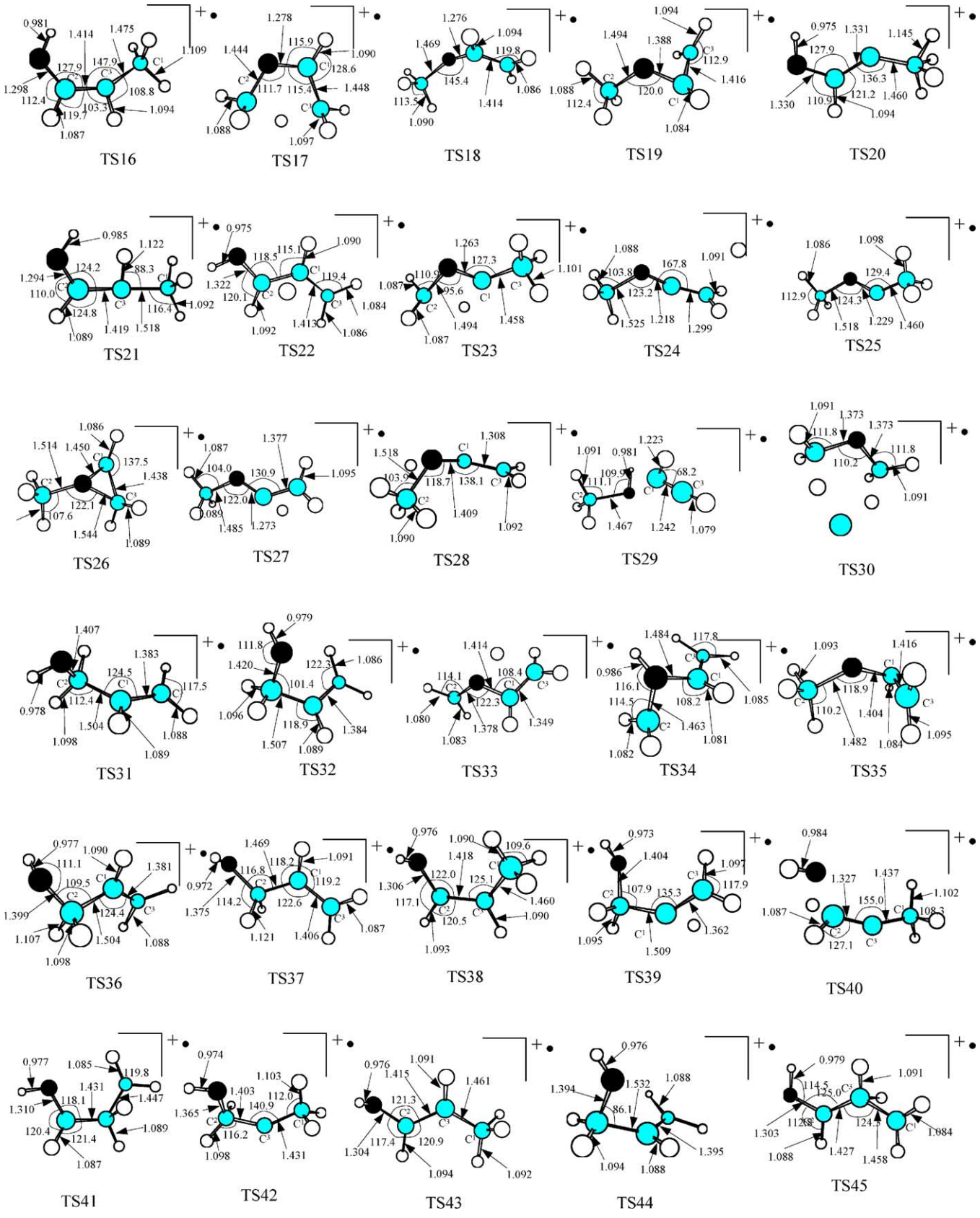

Fig. 2. (*Continued*)

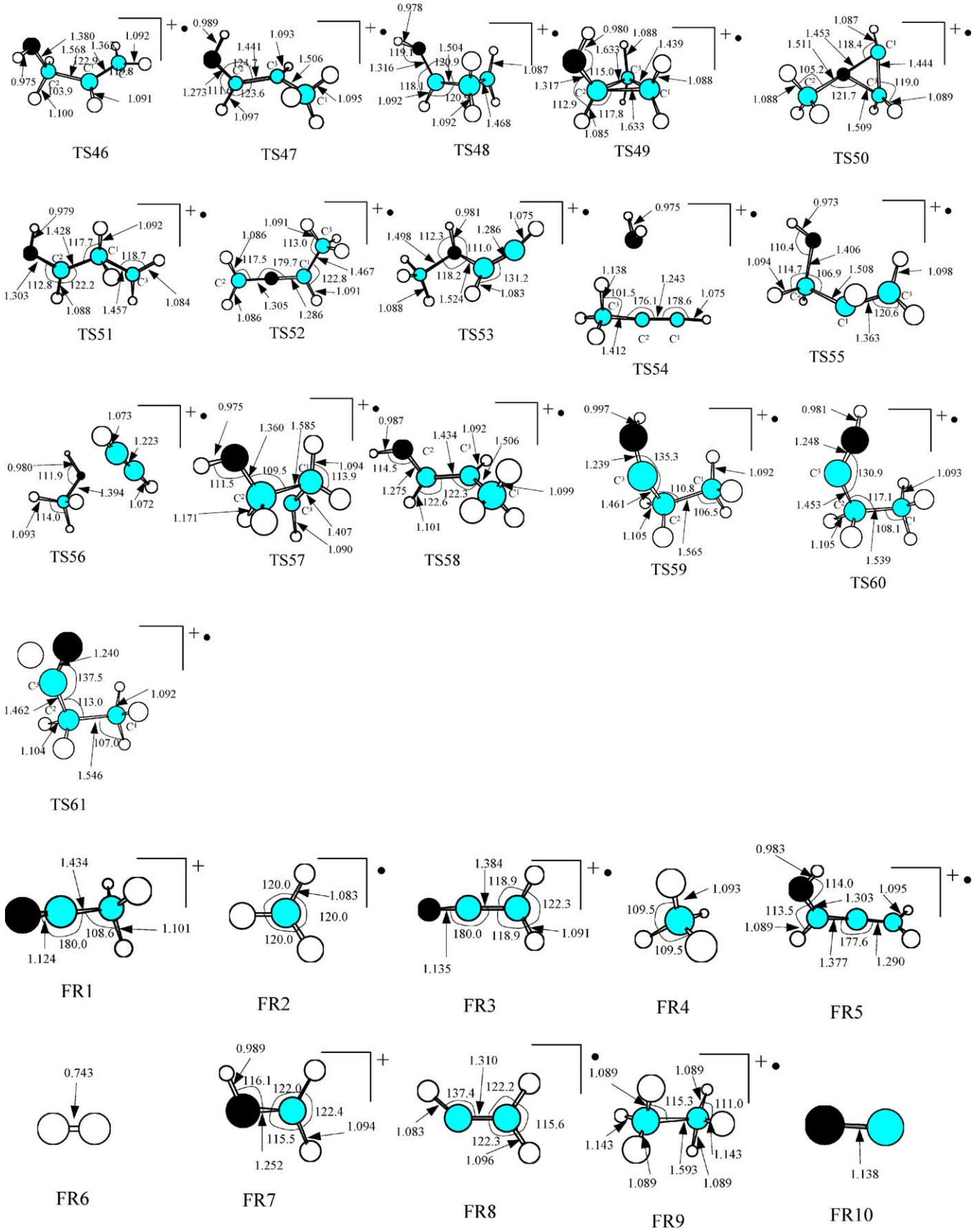

Fig. 2. (*Continued*)

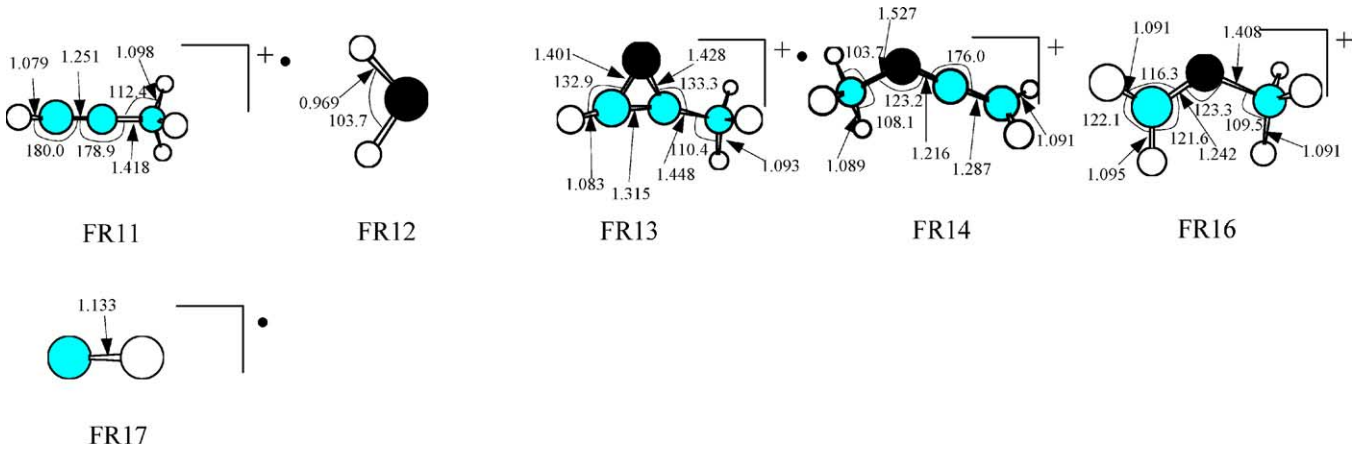

Fig. 2. (*Continued*).

ST5 in Fig. 3 has a pathway other than that leading to the dissociation route (3.d): ST5 → TS7 → ST7. This reaction is ring-opening of the enol tautomer of ST5, keeping the planarity of O–C_2–C_1–C_3 skeleton of the molecule. This simple isomerization is also accomplished by a more involved pathway keeping throughout the enol form, as shown later in Fig. 5.

Another way of transforming ST4 to ST7 is the one-step isomerization ST4 → TS8 → ST7, as shown in Fig. 3. The dihedral angles of O–C^2–C^1–C^3 are −97.463, −44.437, and 0.046° for ST4, TS8, and ST7, respectively. This pathway is lower energetically than that of ST4 → TS4 → ST5 → TS7 → ST7, which means that the one-step isomerization ST4 → TS8 → ST7 is more favorable than the latter.

The reaction (3.f) is the H_2O-elimination of the hydrogen-bridged complex ST33. A hydrogen atom migrates from the methylene group with C^1 to the oxygen atom (ST2 → TS2 → ST3). The resultant H_2O molecule can be easily transferred from C^1 to C^3 along the molecular axis C^1–C^2–C^3 and a hydrogen-bridged complex is formed (ST33). The bond breaking between the H_2O molecule and CH_3CCH^+ takes place with an endothermic energy of 10.78 kcal/mol.

The reaction (3.g) is due to direct elimination of a hydrogen molecule by the reactant ST1. This reaction has

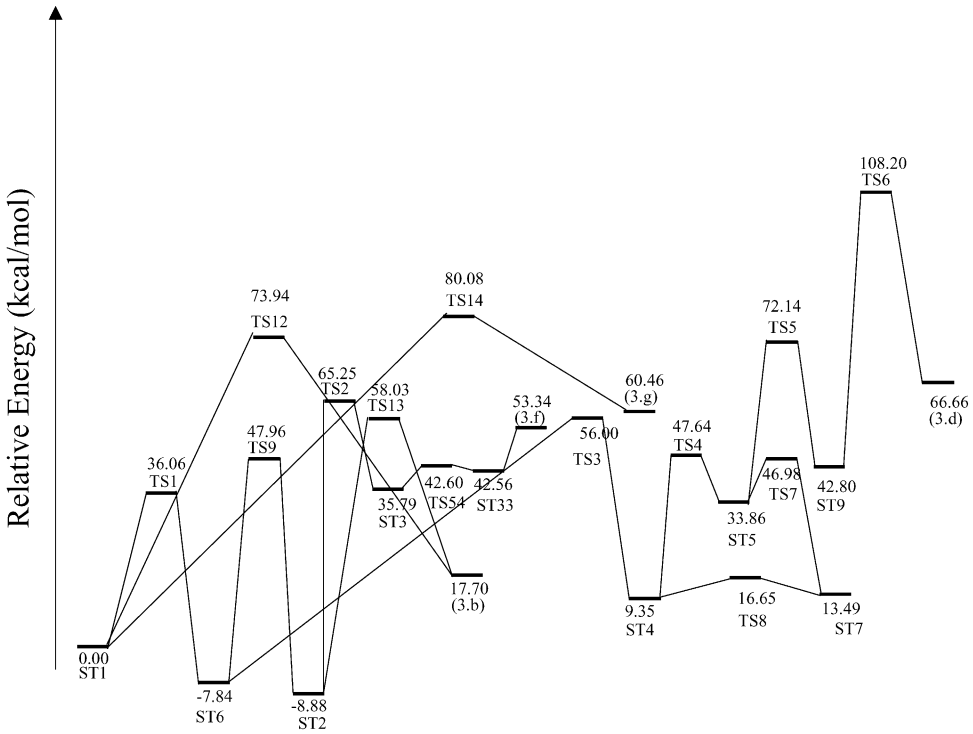

Fig. 3. Potential energy profile for the pathways (3.b), (3.d), (3.f), (3.g), and that to the intermediate ST7 starting from the reactant ST1. Relative energies (in kcal/mol) are calculated by the G2M(cc, MP2) method including the ZPE correction (see text).

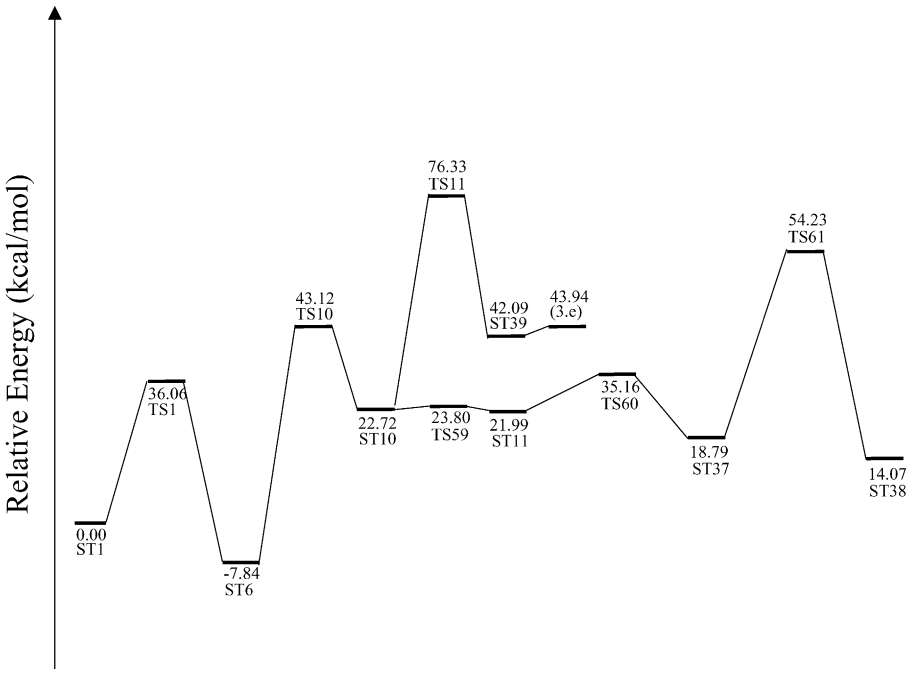

Fig. 4. Potential energy profile for the pathway (3.e). Relative energies (kcal/mol) are calculated by the G2M(cc, MP2) method including the ZPE correction (see text).

the highest potential energy barrier just after the reactant (80.08 kcal/mol). Therefore, this pathway will not contribute so much to the production of the photofragments (3.g). This pathway is only reached with more than nine photons, as is clear from Fig. 1.

From ST2, the reaction (3.b) can take place by the pathway ST2 → TS13 → (3.b) as shown in Fig. 3, although the potential energy barrier is relatively high (66.91 kcal/mol). TS13 is formed by the hydrogen migration from oxygen atom to the methyl group at C^3 of ST2.

Next, we investigate Fig. 4. The unimolecular decarbonylation (3.e) is an endothermic reaction with very low endothermic energy 1.85 kcal/mol for ST39 and is due to the bond breaking of the hydrogen-bridged complexes. The

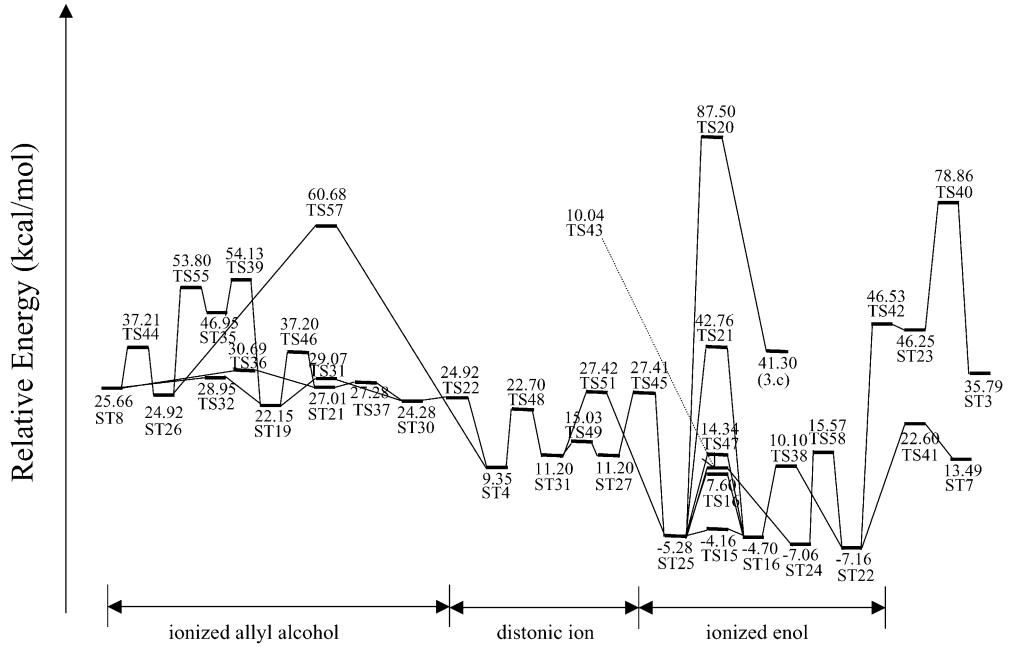

Fig. 5. Potential energy profile for the pathway (3.c) and those to the intermediates ST3 and ST7 starting from the intermediate ST8. Relative energies (kcal/mol) are calculated by the G2M(cc, MP2) method including the ZPE correction (see text).

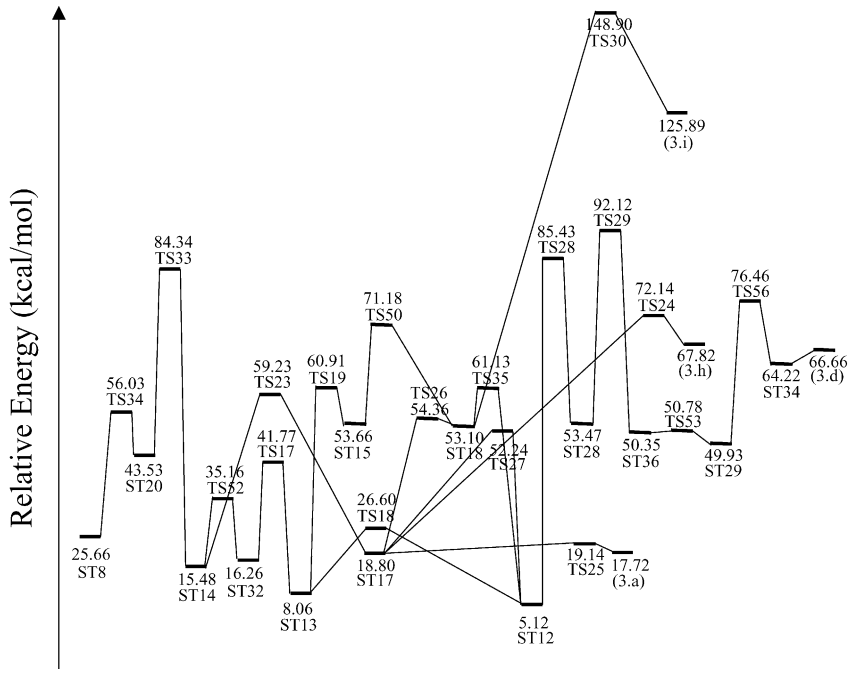

Fig. 6. Potential energy profile for the pathways (3.a), (3.d), (3.h), and (3.i) starting from the intermediate ST8. Relative energies (in kcal/mol) are calculated by the G2M(cc, MP2) method including the ZPE correction (see text).

methyl group at C^1 of ST6 transfers from the carbon atom C^2 to the methylene group at C^3 (ST6 → TS10 → ST10). Following ST10, the hydrogen atom of the enol group forms the hydrogen shifted transition state TS11 from which the hydrogen-bridged ion-neutral intermediate ST39 is produced. ST39 can easily dissociate to produce the cation radical $CH_3CH_3^+$ and neutral CO.

As far as we know, this unimolecular decarbonylation has been investigated in detail only by Hudson et al. [19]. Hudson et al. [19] found that the probability to produce $CH_3CH_3^+$ + CO is much higher than CH_3CH_3 + CO^+ because of the higher energies of the latter. More generally, we have the following possible dissociation products from ST12:

$CH_3CH_3^+ + CO$: 43.94 kcal/mol

$CH_3CH_3^+CO^+$: 102.03 kcal/mol

$CH_3CH_2 + COH^+$: 92.10 kcal/mol

$CH_3CH_2^+ + COH$: 75.77 kcal/mol

$CH_3CH_2 + CO^+ + H$: 199.43 kcal/mol

$CH_3CH_2 + CO + H^+$: 191.87 kcal/mol

$CH_3CH_2^+ + CO + H$: 63.96 kcal/mol

Here, the energies are given relative to that of ST1. From this, we can see that the total energy of $CH_3CH_3^+$ + CO is much lower than that of CH_3CH_3 + CO^+ in the same way as mentioned in [19]. This also holds even if other possibilities given above are taken into account.

Note that our isomerization pathway discussed here is essentially different from that of [19]. ST39 does not correspond to the intermediate **4** of [19] and also we cannot find ST10 and TS11 in [19]. In [19], the reaction pathway was $CH_2CH_2O^+{=}CH_2 \rightarrow CH_3CH_2O^+{=}CH \rightarrow [CH_3CH_2{-}H{-}CO]^+ \rightarrow CH_3CH_3^+ + CO$

Let us investigate the reaction path from ST10 to ST38. The mechanism for the reaction path ST10 → TS59 → ST11 is the rotation of the hydroxy group with C^2–C^3 bond as an axis. The hydroxy group is parallel with C^2–H bond in the case of ST10. However, in the case of TS59, the hydroxy group is directed in the middle of the angle of C^1–C^3–H bond. On the other hand, the hydroxy group is parallel to C^1–C^2 bond in the case of ST11. The isomerization path ST11 → TS60 → ST37 is the rotation of H atom around C^3–O bond. Different from ST11, the hydroxyl group of TS60 is parallel with C^1–H bond, while that of ST37 is parallel with the C^1–C^2 bond. Note that although both of the hydroxyl groups of ST11 and ST37 are parallel with the C^1–C^2 bond, these are directed in the opposite directions. The isomerization path ST37 → TS61 → ST38 is hydrogen transfer from oxygen atom to C^3. This is the same isomerization path with **5** → **1** in [19].

Next, we discuss Fig. 5. The reaction pathway from ST4 to ST7 can be followed by ST4 → TS8 → ST7 in its simplest manner as mentioned above in the text, but a more complicated pathway exists: isomerization process of enol species as shown in Fig. 5. These reaction pathways can be considered as a bypath between ST4 and ST7 of Fig. 3. These isomer-

ization pathways essentially involve a hydrogen shift from one carbon or oxygen atom to another, and rotation of some group as shown below.

Hydrogen atom of C^1 of ST4 migrates to C^2 through TS22 and simultaneously C^1–C^3 bond rotates significantly to produce ST30. The dihedral angles of the bonds O–C^2–C^1–C^3 for ST4, TS22, ST30 are −97.463, −168.559, and −179.944°, respectively. ST4 is also produced from ST26 through TS57. Hydrogen atom of C^3 of ST4 migrates to C^2 which leads to the production of TS57. The bond cleavage of C^1–C^2 of TS57 takes place to yield the bonding C^2–C^3, which leads to the formation of ST26. ST21 and ST30 are related through TS37 by the rotation of the hydroxy group around the O–C^2 bond with very low energy barrier. The ethylene group of ST21 is rotated around the C^1–C^2 bond to form ST19 via the transition state TS46. Note that among the ionized allyl alcohols found in this work, ST19 has the lowest energy, which is consistent with [10]. ST19 and ST30 are also directly connected via TS31 by the rotation of the C^1–C^3 bond around C^1–C^2 bond. The hydrogen atom at C^1 of ST19 migrates to C^3 through TS39 to form ST35. Once again, the hydrogen atom at C^3 of ST35 migrates to C^1 through TS55 to form ST26. Note that ST19 and ST26 are very similar in the energetic viewpoint, but they are different. The dihedral angles for ST19 and ST26 are 0.017 and −81.770°, respectively. ST8 and ST26 are different in that H atoms of the hydroxy group are located on opposite side of the plane defined by O, C^1, and C^2. Hydrogen atom of the hydroxy group of TS44 is found to be in the plane defined above. Note that the enol tautomers originate from ST8 as shown later. In addition to the above pathways, the isomerization from ST21 to ST8 can be realized by only one step through TS36: this is based on the rotation of the plane defined by O, C^1, and C^2 with regard to the bond O–C^2. The pathway from ST4 to ST8 in Fig. 5 mentioned above is the isomerization of ionized allyl alcohol.

ST4 and ST31 are related by rotation of the hydroxy group around the O–C^2 bond. The angle C^2–C^1–C^3 of TS31 decreases and a bond between C^2 and C^3 of ST31 is formed, which leads to the three-membered ring transition state TS49. Then, the bond breaking between C^1 and C^3 of TS49 takes place to produce ST27. Note that ST27 and ST31 are a mirror image for each other and they have the same energy 11.20 kcal/mol. The hydrogen migration from C^3 to C^1 of ST27 takes place and TS45 which is in one plane other than migrating hydrogen atom produces the ionized enol ST25. The isomerization of ST31 to ST25 can also be realized by only one step: in this case, a hydrogen on C^1 of ST31 migrates to C^3 to form ST25 while the dihedral angle of O–C^2–C^1–C^3 decreases from −98.260° to −179.980°. It should be noted that the enol tautomers TS45 and TS51 have the same energy, but they are different in that they are mirror images for each other. The distonic character of ST4, ST31, and ST27 is clear from the Mulliken population analysis: for example, for ST31, the net charge on C^2 is 0.329 and the spin density on C^3 is 1.03, which are the largest among all the atoms. The barrier height for ionized enol ST25 to become distonic ion ST27 or ST31 (32.7 kcal/mol) and the backward one (16.22 kcal/mol) are in reasonable agreement with those of Bouchoux et al. [10].

The isomerization between ST25 and ST16 is a cis-trans transformation. ST25 has trans- and ST16, cis-conformation. The bond C^3–C^1 rotates around C^2–C^3 bond, thereby the dihedral angle O–C^2–C^3–C^1 changing from −179.980° of ST25 to −1.436° of ST16 through −98.990° of TS47. In contrast, the isomerization between ST25 and ST16 through TS16 has little change of the dihedral angle: that of TS16 is −0.212°. This means that the planarity of O–C^2–C^3–C^1 plane is maintained through the reaction ST25 → TS16 → ST16. This also holds for TS15. On the other hand, the bond C^2–C^3–C^1 of TS21 is linear. ST25 and ST24 are related by the rotation of the hydroxy group around the O–C^2 bond. In the same manner, ST16 and ST22 are related by the rotation of the hydroxy group around O–C^2 bond via TS38. ST24 and ST22 are related by the rotation of C^3–C^1 bond around the C^2–C^3 bond through the transition state TS58. Three carbon atoms of ST22, ST24, and TS58 are in one plane, respectively, but the dihedral angles for each one are 0.074, −179.938, and 91.366°, respectively. It should be noted that our results suggest that similarly with [10] ST22 is slightly more stable than ST24 by 0.1 kcal/mol. Note that ST24 is slightly more stable than ST25 by 1.78 kcal/mol, because of the steric repulsion between the hydrogen atom of the hydroxy group and that of C^3. On the other hand, ST22 and ST7 are related by the hydrogen migration between C^1 and C^3. ST22 and ST23 are related by the hydrogen transfer between C^2 and C^3. ST23 and ST3 are related by hydrogen migration from C^2 of ST23 to the O atom. Note that enol radical cations, ST25, ST16, and ST22, are quite stable, as mentioned by Bouchoux et al. [10], the different enol forms, ST2 and ST6, are slightly more stable than the former ones by 2 or 3 kcal/mol. As discussed by Bouchoux et al. [10], comparing the energies of ST16 and ST22, ST22 is slightly more stable than ST16 by 2.46 kcal/mol due to the preference for hydroxylic hydrogen to be anti with respect to the CC double bond.

The reaction (3.c) stems from ST25 and is the direct elimination of the hydrogen molecule after the many-step isomerization of the reactant as shown in Fig. 5. In this case, the energy barrier is very high because the transition state TS20 has a high energy (87.50 kcal/mol).

Next, we concentrate on Fig. 6. The transition state TS34 in this figure plays a key role to connect the enol and the ether forms. The methyl vinyl ether cation radical is produced by migration of vinyl group (CH_2=CH–) from the carbon atom C^2 to the oxygen atom (ST8 → TS34 → ST20). In particular, the investigation of rotational isomerism in vinyl ethers is of considerable interest [20]. The hydrogen atom attached to the oxygen atom of ST20 migrates to C^1 to form ST14 with a high energy barrier (40.81 kcal/mol). The trans form (ST14) is slightly more stable than the cis form (ST32). Because the methyl group and the methylene group are close, hydrogen transfer takes place between them. As a result, the cis-methyl

vinyl ether cation radical is produced (ST13). The methylene group of ST13 rotates around the C^1–O axis and ST15 is formed. ST14 and ST17 are related by the migration of the hydrogen atom combined with C^1 of ST14 to C^2 of ST14 to form ST17. ST17 and ST18 are also related by hydrogen transfer from C^3 of ST17 to C^1 to form ST18. ST15 and ST18 are related by rotation of C^1–C^3 bond around the O–C^2 axis. ST18 and ST12 are related by the rotation of CH_2CH group around the O–C^2 axis. ST17 and ST12 are also connected only by the hydrogen transfer via TS27. ST12 and ST28 are related by the hydrogen migration of C^1 to the oxygen atom by a high energy barrier (80.31 kcal/mol). ST36 is produced by migration of C^3 to the oxygen atom of ST28. ST36 and ST29 are related by the rotation of HCCH unit around the axis defined by the line between the O atom and the C atom of HCCH. Then, the bond between the C atom of HCCH and the O atom of CH_3OH is cleaved, and the HCCH unit transfers to form hydrogen bridging between the C atom of HCCH and the C atom of CH_2OH. Finally, the hydrogen bridging is split endothermically with 2.44 kcal/mol barrier to form CH_2OH^+ + CH_2CH (3.d).

From ST18, a very high energy transition state TS30 can be formed, and photofragments $CH_3OCH_2^+$ and CH are produced (3.i). The pathway (3.i) has the highest transition state in the present work so it may contribute to the photodissociation the least. In addition, from ST17, one-hydrogen elimination is possible via the high energy transition state TS24 (72.14 kcal/mol): (3.h). ST17 also undergoes direct bond breaking between the methyl group and O atom: (3.a).

This direct bond breaking of ST17 was discussed experimentally by Lifshitz [21] and by Turecek and McLafferty [22]. ST12 corresponds to the intermediate methyl vinyl ether cation radical *e* and ST17 to the intermediate *f* in [21], or ST12 to *b* and ST17 to *c* in [22]. In addition, the dissociation pathway ST12 → TS27 → ST17 → TS25 → (3.a) corresponds to that of $e \rightarrow f \rightarrow CH_3CO^+ + CH_3$ in Scheme 2 of [21] or $b \rightarrow c \rightarrow CH_3CO^+ + CH_3$ in Scheme 1 of [22].

Some comments about the results of the ab initio calculations mentioned above are in order.

Firstly, it was pointed out that hydrogen-bridged species play roles as intermediates in decompositions of simple carbonyl compounds and that their formation can take place only below their respective thresholds of decomposition (endothermic reaction) [4,23]. In the present study, this is also the case for the reactions (3.e) in Fig. 4 and (3.f) in Fig. 3 besides (3.a) and (3.b) which are not presented in the present work. The reactions (3.d) and (3.i) in Fig. 3 are the exceptions.

Secondly, as was mentioned above, in general, the enol tautomers ST16, ST24, and ST25 in Fig. 5 are quite stable in accord with [4]; they have lower energies than the reactant ST1 in Fig. 3. The enol tautomers ST4 and ST7 in Fig. 3, and ST8, ST19, ST21, ST22, ST26, ST27, ST30, and ST31 in Fig. 5 are also very stable, but they have a slightly higher energies than the reactant ST1 in Fig. 3 (also see Table 1).

Thirdly, from the present calculation, it is revealed that ST2 in Fig. 2 has the lowest energy. It is not necessarily ST30 in Fig. 5 (*Z*-prop-1-en-1-ol) which Bouchoux et al. [10] claimed that it is the most stable ionic structure among the isomers of $C_3H_6O^+$ cation radical.

Finally, methyl and methane losses from the acetone cation radical are the only dissociations of that ion just above their thresholds, but this is not the case at higher energies. An examination of a 70 eV electron impact mass spectrum of the acetone cation radical reveals many other products, including low abundance species corresponding to most of (3.c)–(3.i).

4. Conclusions

We have performed high level ab initio (using Gaussian-2 (G2M) method) calculation for the reactant, intermediates, transition states, and photofragmentation products of the $C_3H_6O^{+\bullet}$ cation radical in order to elucidate its unimolecular photofragmentation and isomerization mechanism in an intense laser field. The dissociation pathway from TS1 in Fig. 3, one of the local minima found by but not studied in detail Heinrich et al. [4], was found to be the cornerstone of the new channels in this study. This is because if we assume that the acetone cation radical ST1 in Fig. 3 is the initial state, the transition pathway from ST6 which is connected to ST1 by TS1 leads to almost all of the isomers in Figs. 3–6. We have found that there should be many pathways that are capable to produce other important isomerization and photodissociation products. Particularly, it was found that keto-enol isomerization is important and involved for ketones. This was, for example, verified by the thermal dissociation of several substituted acetophenone molecular ions studied experimentally and theoretically by Giroldo et al. [24]. However, it was assumed that the isomers found in this work hardly contribute to the photodissociation products at the steady state limit.

Finally, it should be mentioned that it will also be possible that the singly charged photofragment cations found in this study decompose further to produce smaller photofragments by unimolecular reactions [16].

Acknowledgments

The authors wish to thank Academia Sinica, National Science Council of ROC for supporting this work. K. Mishima would like to thank Dr. A.M. Mebel for useful discussions.

References

[1] D.J. McAdoo, F.W. McLafferty, J.S. Smith, J. Am. Chem. Soc. 92 (1970) 6343;
J.H. Beynon, R.M. Caprioli, R.G. Cooks, Org. Mass Spectrom. 9 (1974) 1;
C.C. van de Sande, F.W. McLafferty, J. Am. Chem. Soc. 97 (1975) 4617;
D.J. McAdoo, D.N. Witiak, J. Chem. Soc. Perkin 2 (1981) 770;
C. Lifshitz, Int. J. Mass Spectrom. Ion Phys. 43 (1982) 179;

F.W. McLafferty, D.J. McAdoo, J.S. Smith, R. Kornfeld, J. Am. Chem. Soc. 93 (1971) 3720;
J. Diekman, J.K. MacLeod, C. Djerassi, J.D. Baldeschwieler, J. Am. Chem. Soc. 91 (1969) 2069;
I. Powis, C.J. Danby, Int. J. Mass Spectrom. Ion Phys. 32 (1979) 27;
R. Stockbauer, Int. J. Mass Spectrom. Ion Phys. 25 (1977) 89;
D.J. McAdoo, C.E. Hudson, Int. J. Mass Spectrom. Ion Phys. 59 (1984) 77;
G. Bouchoux, Y. Hoppilliard, Can. J. Chem. 60 (1982) 2107;
A.J. Stace, A.K. Shukla, Int. J. Mass Spectrom. Ion Phys. 37 (1981) 35;
W.J. van der Sande, D.P. deBruijn, J. Loss, P.G. Kistemaker, S.A. McLuckey, Int. J. Mass Spectrom. Ion. Phys. 67 (1985) 161;
P.J. Derrick, S. Hammerum, Can. J. Chem. 64 (1986) 1957;
R. Bombach, J.P. Stadelmann, J. Vogt, Chem. Phys. 72 (1982) 259;
A.K. Shukla, K. Qian, S.L. Howard, S.G. Anderson, J.H. Futrell, Int. J. Mass Spectrom. Ion. Proc. 92 (1989) 147;
C. Lifshitz, J. Phys. Chem. 87 (1983) 2304;
K. Qian, A. Shukla, S. Howard, S. Anderson, J. Futrell, J. Phys. Chem. 93 (1989) 3889;
C. Majumder, O.D. Jayakumar, R.K. Vatsa, S.K. Kulshreshtha, J.P. Mittal, Chem. Phys. Lett. 304 (1999) 51;
J.A. Nummela, B.K. Carpenter, J. Am. Chem. Soc. 124 (2002) 8512.

[2] C.S.T. Cant, C.J. Danby, J.H.D. Eland, J. Chem. Soc., Faraday Trans. II 71 (1975) 1015;
D.M. Mintz, T. Baer, Int. Mass Spectrom. Ion Phys. 25 (1977) 39;
I. Powis, C.J. Danby, Int. Mass Spectrom. Ion Phys. 32 (1979) 27;
C. Lifshitz, E. Tzidony, Int. Mass Spectrom. Ion Phys. 39 (1981) 181.

[3] D.J. McAdoo, Mass Spectrom. Rev. 19 (2000) 38.

[4] N. Heinrich, F. Louage, C. Lifshitz, H. Schwarz, J. Am. Chem. Soc. 110 (1988) 8183.

[5] M.D. Ceno, A.G. Lafont, J.M. Lluch, J. Bertran, Mol. Phys. 92 (1997) 393.

[6] W.M. Jackson, D. Xu, J. Chem. Phys. 113 (2000) 3651.

[7] L.V. Keldysh, Sov. Phys. JETP 20 (1965) 1307.

[8] K. Mishima, M. Hayashi, J. Yi, S.H. Lin, H.L. Selzle, E.W. Schlag, Phys. Rev. A 66 (2002) 033401;
K. Mishima, M. Hayashi, J. Yi, S.H. Lin, H.L. Selzle, E.W. Schlag, Phys. Rev. A 66 (2002) 053408.

[9] C. Wu, Y. Xiong, N. Ji, Y. He, Z. Gao, F. Kong, J. Phys. Chem. A 105 (2001) 374.

[10] G. Bouchoux, A. Luna, J. Tortajada, Int. J. Mass Spectrom. Ion. Proc. 167–168 (1997) 353.

[11] V.R. Bhardwaj, D.M. Rayner, D.M. Villeneuve, P.B. Corkum, Phys. Rev. Lett. 87 (2001) 253003.

[12] A.D. Becke, J. Chem. Phys. 98 (1993) 5648;
C. Lee, W. Yang, R.G. Parr, Phys. Rev. B 37 (1988) 785.

[13] A.M. Mebel, K. Morokuma, M.C. Lin, J. Chem. Phys. 103 (1995) 7414.

[14] L.A. Curtiss, K. Raghavachari, G.W. Trucks, J.A. Pople, J. Chem. Phys. 94 (1991) 7221;
J.A. Pople, M. Head-Gordon, D.J. Fox, K. Raghavachari, L.A. Curtiss, J. Chem. Phys. 90 (1989) 5622;
L.A. Curtiss, C. Jones, G.W. Trucks, K. Raghavachari, J.A. Pople, J. Chem. Phys. 93 (1990) 2537.

[15] M.J. Frisch, G.W. Trucks, H.B. Schlegel, G.E. Scuseria, M.A. Robb, J.R. Cheeseman, V.G. Zakrzewski, J.A. Montgomery Jr., R.E. Stratmann, J.C. Burant, S. Dapprich, J.M. Millam, A.D. Daniels, K.N. Kudin, M.C. Strain, O. Farkas, J. Tomasi, V. Barone, M. Cossi, R. Cammi, B. Mennucci, C. Pomelli, C. Adamo, S. Clifford, J. Ochterski, G.A. Petersson, P.Y. Ayala, Q. Cui, K. Morokuma, D.K. Malick, A.D. Rabuck, K. Raghavachari, J.B. Foresman, J. Cioslowski, J.V. Ortiz, A.G. Baboul, B.B. Stefanov, G. Liu, A. Liashenko, P. Piskorz, I. Komaromi, R. Gomperts, R.L. Martin, D.J. Fox, T. Keith, M.A. Al-Laham, C.Y. Peng, A. Nanayakkara, C. Gonzalez, M. Challacombe, P.M.W. Gill, B.G. Johnson, W. Chen, M.W. Wong, J.L. Andres, M. Head-Gordon, E.S. Replogle, J.A. Pople, Gaussian, Inc., Gaussian 98 (Revision A.9), Pittsburgh, PA, 1998.

[16] F.W. McLafferty, Interpretation of Mass Spectra, University Science Books, Mill Valley, California, 1980.

[17] W.J. Bouma, J.K. MacLeod, L. Radom, J. Am. Chem. Soc. 102 (1980) 2246.

[18] F. Turecek, C.J. Cramer, J. Am. Chem. Soc. 117 (1995) 12243, references therein.

[19] C.E. Hudson, D.J. McAdoo, J.C. Traeger, J. Am. Soc. Mass Spectrom. 13 (2002) 1235.

[20] A.V. Abramov, A.V. Vashchenko, Yu. L. Frolov, J. Mol. Struct. (Theochem.) 594 (2002) 101.

[21] C. Lifshitz, Org. Mass Spectrom. 23 (1988) 303.

[22] F. Turecek, F.W. McLafferty, J. Am. Chem. Soc. 106 (1984) 2528.

[23] N. Heinrich, J. Schmidt, H. Schwarz, Y. Apeloig, J. Am. Chem. Soc. 109 (1987) 1317;
T. Drewello, N. Heinrich, W.P.M. Maas, N.M.M. Nibbering, T. Weiske, H. Schwarz, J. Am. Chem. Soc. 109 (1987) 4810;
N. Heinrich, H. Schwarz, Int. J. Mass Spectrom. Ion Proc. 79 (1987) 295.

[24] T. Giroldo, J.M. Riveros, J. Phys. Chem. A 106 (2002) 9930.